# Active noise control on a BOSE headset

# Active Noise Control on a BOSE® headset

R.M.L. Ellenbroek
B.H.M. Bukkems
DCT report: 2002-23

Eindhoven, March 2002

R.M.L. Ellenbroek, student id. 446352
B.H.M. Bukkems, student id: 428119

Coach: Prof. dr. ir. R.A. de Callafon
Prof. dr. ir. M. Steinbuch

# Abstract

This paper on Active Noise Control (ANC) presents the modelling and digital control of a BOSE ® headset. This headset is equipped with a microphone in front of the speaker inside the earcup. With the use of this speaker and microphone, a feedback loop can be constructed. In order to design a feedback controller, models of the system dynamics and the noise filter are derived. Using a controller relevant modelling step, the performance of the initially designed feedback controller is improved. The adjustability of the noise reducing area is investigated by varying one of the weighting filters used. This results in a digital controller that is capable of reducing noise in specific frequency areas. Finally, experiments have shown that the system dynamics are dependent on the person wearing the headset, possibly resulting in stability problems.

# 1. Introduction

For many years people have been trying to reduce sound and vibration noises generated by a variety of different sources, like engines [1], fans or other devices. This can be done passively or actively, where the passive reduction of noise is generally realised by inserting sound isolating materials. The more complex, active method – known as *active noise cancellation* (*ANC*) – requires sensors, control circuitry and actuators. The advantage of the active approach is that the same noise reduction can be achieved with lighter constructions, and is more adjustable and practical to use. Examples of successful implementations of *ANC* can be found in helicopter/airplane headsets, MRI scanners [2], ducts in for example air-conditioning systems [3], etc.
The effort of noise reduction can be made at both the noise generating side and at the noise receiving side, i.e. the human ear. Although a lot of research is currently being done to reduce noise production of many machines and devices, there are still many environments that have high noise levels, for example in construction work area's, helicopters and airplanes, but also in spaces with lower background noises – for example inside cars – human concentration is reduced because of this noise. In this respect, the 'hearing side' is an effective position to attempt noise reduction.
Active noise cancellation has been studied for many years, using many different control techniques. Feedforward [4] as well as feedback [5] and hybrid techniques have proven their values. Synthesis techniques applicable to ANC include LQG [3], $H_2$ and $H_\infty$ [6]. Recently, the audio equipment company BOSE® has released a headset featuring analogue filtering circuitry to achieve active noise reduction [11].
In this project, $H_2$ feedback control techniques were applied to this commercial headset, realising relative silence inside the ear cups by cancelling outside noises. However, instead of using analogue circuitry, a digital controller is used.
Generally, control or filter design has been based on physical models of the regarding systems, as shown in [7], where many simplifications are made that are potentially harmful to the controller performance. In this project, controller relevant system identification is done to obtain the transfer functions of dynamical systems on which the controller is to be based. This way, a relatively low order model was found to be rich enough to be used to design a controller with sufficient noise reduction.
Due to advances in computing power, it has become possible to use digital techniques to implement the designed controllers. Despite the theoretical advantages of analogue filters, their digital counterparts are much better suited for research applications. They are much easier to adjust or change and can still be commercially viable when using fast DSP-chips [8]. In order to exploit this advantage to the fullest, an attempt is also made to create a controller that can achieve noise reduction over an easily adjustable, but limited frequency range.

In the course of this paper, first the experimental set-up will be discussed, followed by the synthesis of the models necessary for controller synthesis. On the basis of these results a controller will then be computed and implemented into the real system. The controller can now be evaluated and the measured sensitivity function can be compared to the calculated sensitivity function. Using the difference between these functions, the controller can be improved in an iterative process, called 'controller relevant modelling'.
Next, effort will be made to use weighting functions to place the effective bandwidth in a desired area; thus moving the effective noise reduction zone over the frequency axis. Depending on the results, an adjustable controller may then be parameterised.
Before a final conclusion will be drawn, the results of transfer function measurements on real people will be shown and their implications discussed.

# 2. Experimental set-up and approach

## 2.1. BOSE® active headset

A modified BOSE® active headset, that was originally designed for noise reduction purposes makes up the basis of the experimental set-up used in this project. A picture of the inside of the ear cups of this headset can be found in figure 2-1. This headset already has a microphone inside the ear shell, generating a signal suitable for feedback-control. However, in order for the headset to be usable for noise cancellation research, the analogue circuitry responsible for the noise cancellation had to be removed whereas an external amplifier was added to adjust the amplitude of the incoming and outgoing signals to be compatible with the required D/A and A/D converters.

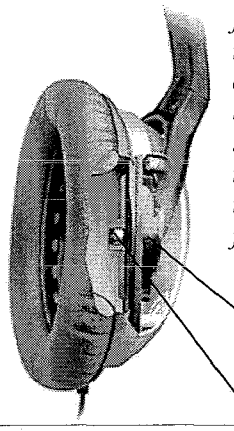


*figure 2-1: The insides of an ear cup of the used bose-headset. Note that the microphone is positioned centered directly in front of the speaker.*

In order to get the best consistent results, the headset is placed on a dummy head inside a sound-isolated box. This way, the measurements are least disturbed with environment noise. Environment noise can then be generated – if needed – by an external speaker, and measured by an external microphone. A schematic of the experimental set-up can be seen in figure 2-2.

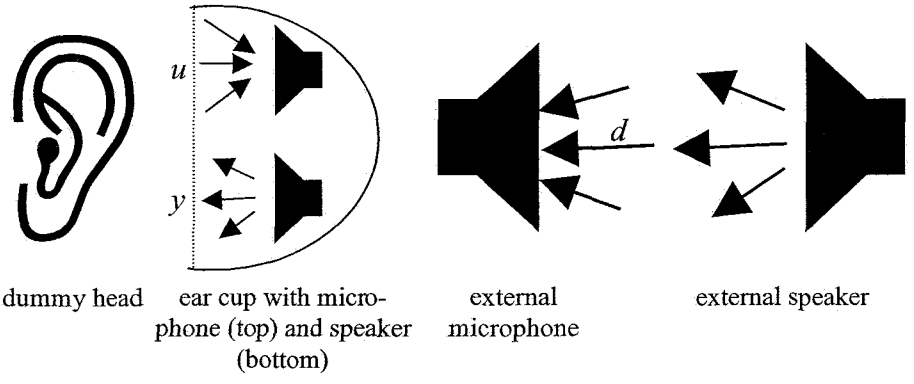


*figure 2-2: A schematic representation of the experimental set-up.*

## 2.2. Schematics

A schematic of the experimental set-up can be made as depicted in figure 2-3. The plant $G$ represents the dynamical system acting between the speaker and the microphone inside the ear cup. The noise filter $H$ represents the dynamical system made up by the ear cup acting between the environment and a listener's ear. The noise filter $H$ is thus the passive noise reduction achieved by the ear cups of the headset. The signals $u$, $d$ and $y$ are the input of the system $G$, the noise disturbance and the output of the system respectively.

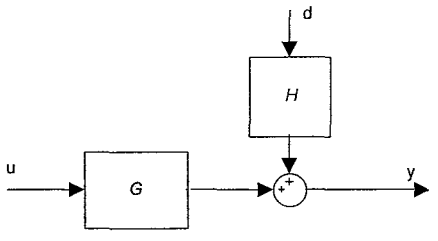


*figure 2-3: The schematic structure of the system.*

## 2.3. Data acquisition

In order to be able to estimate the plant and noise model, $G_m$ and $H_m$ respectively, two experiments have been conducted. First, the plant $G$ was measured by injecting (band limited) white noise into the speaker inside the ear cup – thus exciting the plant $G$ - and measuring the response-signal of the microphone inside the ear cup to this signal. From these two measured signals, an empirical transfer function estimate can be calculated.
The second relevant system is the noise filter $H$. In order to obtain measurements of this filter, the following experiment was conducted: the external speaker, attached to an amplifier was used to create noise. Because the noise from the noise generator is fed through an amplifier and a speaker – both dynamical systems acting on the signal – the sound outside the ear cup is different from the generated noise signal. In order to exclude the amplifier- and (external) speaker-dynamics from the measured noise filter $H$, the noise outside the ear cup is measured with an external microphone (see figure 2-2) while the microphone inside the ear cup measures the noise inside the ear cup. From the two measured signals an empirical transfer function estimate can be calculated.

## 2.4. Approach to ANC

The first step in designing a feedback controller for Active Noise Control is the estimation of the headset dynamics, i.e. estimation of the plant $G$, and estimation of the noise model dynamics, i.e. estimation of the noise filter $H$. Both models are estimated using curve fitting techniques and are described in sections 3.2 and 3.3 respectively. Once these models have been found, an $H_2$ optimal controller is computed in a process that is described in section 4. Once this controller is computed, it is used in a controller relevant modelling design step, in which the model of the plant $G$ is improved. This design step is described in the sections 3.4 and 5.1. Finally a new $H_2$ optimal controller is computed, using the new model of the plant $G$. Using this controller, the sensitivity function $S$, which shows the amount and frequency domain of noise reduction, is evaluated, as described in section 5.2. Because the model of the noise filter $H$ has a lot of influence on the shape of the controller (see section 4.4), it is used to adjust the controller, with the result that the area of noise reduction changes. This is described in section 6. Finally, section 7 discusses issues of applying the headset to real people.

# 3. Model estimation

In this section an explanation of the model-synthesis techniques used is described, as well as the estimated models for the dynamical systems as measured in section 2.3, i.e. $G$ and $H$.

## 3.1. Curve fitting

The parameterisation technique used for model synthesis is called 'curve fitting'. This technique fits a continuous time transfer function of arbitrary order to a given set of measurement data. The fit-criterion used is the minimization of the weighted 2-norm of the estimation error. Let the measurement data to be parameterised be

$$G = \{G(\omega) \mid G(\omega) \in C^{1\times N}\} \tag{3-1}$$

where the frequency response data is evaluated along a frequency grid

$$\omega \in \Omega := \{\omega_k, for\, k = 1,2,\ldots N\} \tag{3-2}$$

at $N$ frequency points.
In the case of this project, the dynamical systems to be parameterised are both Single-Input Single-Output (SISO) systems, so that the model $P(\omega,\theta)$ can be written in transfer function format as the fraction of two polynomials $A$ (monic) and $B$:

$$P(\omega,\theta) = \frac{\mathrm{B}(\omega,\theta)}{A(\omega,\theta)} = \frac{b_0 + b_1 s + b_2 s^2 + \ldots + b_{nb-1} s^{nb-1}}{1 + a_1 s + a_2 s^2 + \ldots + a_{na} s^{na}} \tag{3-3}$$

where

$$s = j\omega \tag{3-4}$$

and

$$\theta = [a_1, a_2, \ldots, a_{na}, b_0, b_1, \ldots, b_{nb-1}]^T \tag{3-5}$$

is the unknown parameter to be estimated, and $na$ and $nb$ are the number of parameters in the $A$- and $B$-polynomial respectively.
The curve-fit is calculated by minimizing the 2-norm of the estimation error over the frequency grid $\omega$:

$$\theta = \arg\min_{\theta\in\mathbf{R}} \left\| W(\omega)\left(G(\omega) - P(\omega,\theta)\right)\right\|_2 \tag{3-6}$$

where $W(\omega)$ is a weighting function and $G(\omega)$ is the measured frequency response data of the plant $G$. The weighting function is very important, because it specifies where the measurement data should be fitted accurately. Although the absolute minimum of the 2-norm is always 0 and lies where the model $P$ equals the measurement data $G$, this minimum will practically never be reached. Moreover, because of its logarithmic character, many details of a transfer functions exist in small magnitudes, thus requiring some kind of relative error weighting in order to be fitted sufficiently. This can be achieved by choosing

$$W(\omega) = G^{-1}(\omega). \tag{3-7}$$

## 3.2. Estimation of headset dynamics

First, low ($6^{th}$) order models have been estimated upon the measurement data using a weighting function based on the inverse of the measurement data (see equation 3-7). In subsequent steps,

adjusting the weighting function and/or supplying more freedom by increasing the number of model-parameters to be estimated enhanced these model estimates.
However, since it is at this point not yet known which resonance modes will prove to be important for performance or closed loop stability, only a generally accurate model can be estimated. After a controller has been implemented, closed loop measurements provide better ways to estimate the plant model $G_m$, as described in section 3.4 and 5.1.
The initial estimate of $G$ used for controller synthesis is a $10^{th}$ order fit, plotted together with the measurement data in figure 3-1.

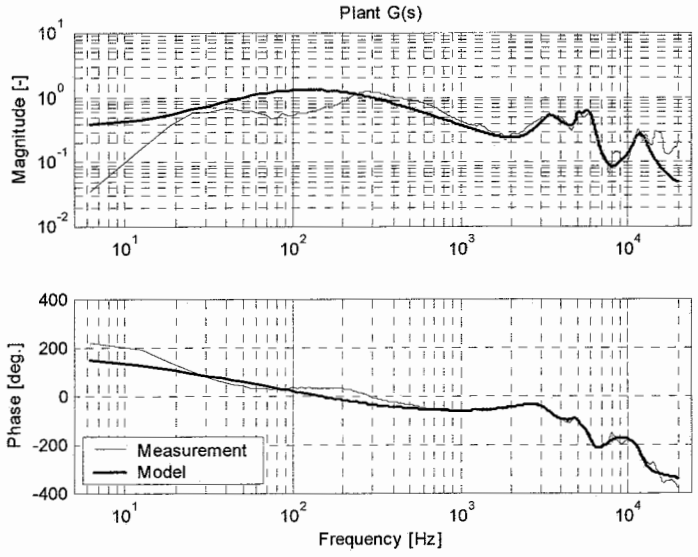


*figure 3-1: Amplitude and phase plot of the plant measurement G (thin line) together with the estimated $10^{th}$ order model $G_m$ (thick line).*

## 3.3. Noise model dynamics

The purpose of the model estimation of the noise model $H_m$ is quite different than for the plant $G$. For $G$, an accurate fit is essential to performance and closed-loop stability. However, since $H$ is not part of the closed loop, it has a different effect on the closed loop system.
The noise filter $H$ more or less defines where noise to be suppressed exists. Because $H$ is present in the augmented plant, it acts as a weighting function and therefore it shapes the resulting controller.
As a result of this, it is useless to estimate an accurate (high order) model for $H$; doing so would only result in a high order and therefore complex controller. Instead, several other methods to derive an appropriate noise filter $H$ have been used.

1. A low order estimate, acquired by reducing a high order estimate.
   By using the same estimation routine as for the plant $G$, a $10^{th}$ order estimate was obtained. Using model-state-reduction techniques, it has been reduced to a $4^{th}$ order filter. The $4^{th}$ (reduced) order fit of $H$ found with this method will be used in the next section for controller synthesis. A plot of both models can be found in figure 3-2, together with the measurement data of the noise filter $H$.
2. A pole-placement procedure, creating a hat shaped noise filter with the same maximum magnitude as the measurement data of $H$. This method of creating custom filters will be used in section 6, when the peak in the noise filter is moved along the frequency axis.

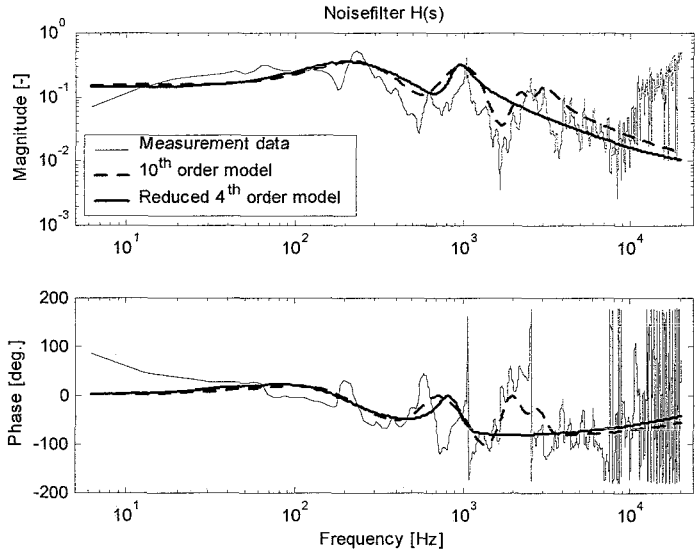


*figure 3-2: Amplitude and phase plot of the noise filter measurement H (thin line) together with the 10th (dotted line) and reduced 4th (thick line) order models. Note the measured magnitude tends to increase for high frequencies as a result of measurement noise, while in fact it should decrease.*

## 3.4. Controller relevant modeling

The second step in the estimation of the model $G_m$ of the plant $G$ is controller relevant modeling. Once a controller has been computed, which is based on the initial model of the plant $G$, this controller can be used to improve $G_m$ in an iterative process. With the use of this improved model, a new controller can be computed which, after implementing, will lead to a model sensitivity that looks more like the measured sensitivity.

In order to improve $G_m$, a second fit of the plant $G$ is made, using the same techniques as described in section 3.1, but with a different weighting function. This weighting function consists of two parts. The first part is the model $H_m$ of the noise filter $H$,

$$W_1(\omega)=H_m(\omega) \tag{3-8}$$

since this model plays an important role in the calculation of the controller (see section 4.4) and therefore in the calculation of the resulting sensitivity function. The second part of the weighting function comes from the fact that the sensitivities computed from the model $G_m$ and the measurement data of the plant $G$, are desired to be the same. To make the difference between these two sensitivities as low as possible, its 2-norm is minimized:

$$\begin{aligned}
&\left\| \left( \frac{1}{1-G_m(\omega)K(\omega)} \right) - \left( \frac{1}{1-G(\omega)K(\omega)} \right) \right\|_2 \\
&= \left\| \left( \frac{K(\omega)}{(1-G_m(\omega)K(\omega))(1-G(\omega)K(\omega))} \right) (G_m(\omega)-G(\omega)) \right\|_2 \\
&= \| W_2 (G_m(\omega)-G(\omega)) \|_2
\end{aligned} \tag{3-9}$$

In equation (3-9), $G_m(\omega)$ represents the new model of the plant $G$, but since this model is not known yet, the initial model is used, assuming that the difference between these models is small. The used weighting function for the improvement of the model of the plant $G(\omega)$ is shown in equation (3-10):

$$W = W_1 W_2 = \frac{H_m(\omega)K(\omega)}{(1 - G_m(\omega)K(\omega))(1 - G(\omega)K(\omega))} \tag{3-10}$$

The results of this controller relevant modeling technique are discussed in section 5.1.

# 4. Control design

This section shows the design proces of the $H_2$ controller $K$, the way of discretizing the controller and the resulting noise reduction based on the fits of the plant $G$ and the noise filter $H$.

## 4.1. The general $H_2$ control problem configuration

The block diagram depicted in figure 4-1 is the general configuration of an $H_2$ control problem. In this block diagram, $P$ is the augmented plant and $K$ is the controller. Furthermore, $\underline{w}$ is the vector with exogenous input signals and $\underline{z}$ is the vector with the so-called 'error' signals to be minimized to meet the control objectives. $\underline{u}$ is the vector with control variables and $\underline{y}$ is the vector with measured outputs.

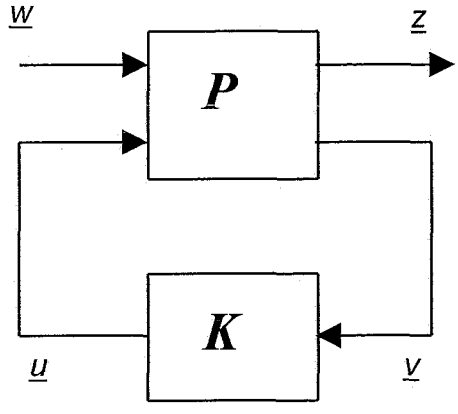


*figure 4-1: The standard block diagram.*

The system of figure 4-1 is described by the following matrix equations:

$$\begin{bmatrix} z \\ y \end{bmatrix} = P \cdot \begin{bmatrix} w \\ u \end{bmatrix} = \begin{bmatrix} P_{11} & P_{12} \\ P_{21} & P_{22} \end{bmatrix} \cdot \begin{bmatrix} w \\ u \end{bmatrix} \tag{4-1}$$

$$u = K \cdot y \tag{4-2}$$

These matrix equations are valid for both the continuous as the discrete time case. In this project, controller design has been done in continuous time because of the simplicity of the equations. When the controller has to be implemented into the system, it will be converted to discrete time (see section 4.6).

The state-space realization of the transfer matrix $P$[1)] is taken to be of the following form:

$$P = \begin{bmatrix} A & B \\ C & D \end{bmatrix} = \left[\begin{array}{c|cc} A & B_1 & B_2 \\ \hline C_1 & D_{11} & D_{12} \\ C_2 & D_{21} & D_{22} \end{array}\right] = \left[\begin{array}{c|cc} A & B_1 & B_2 \\ \hline C_1 & 0 & D_{12} \\ C_2 & D_{21} & 0 \end{array}\right] \tag{4-3}$$

It can be seen that $D$ has a special off-diagonal structure. $D_{11}$ is assumed to be zero in order to guarantee that the $H_2$ problem is properly posed. That means that under the assumption $D_{11} = 0$,

---

1) *Considering the continuous time case, the matrices used are a function of s, but for simplicity the s is left out.*

the transfer function $P_{11}$ is strictly proper[2]. $D_{22}$ is assumed to be zero so that $P_{22}$ is strictly proper and the formulas in the $H_2$ algorithm are simplified.
For the output feedback control $H_2$ problem, four assumptions are made (see also [9]):

(i) $(A, B_2)$ is stabilizable and $(C_2, A)$ is detectable. The first part of this assumption implies that the matrix $\begin{bmatrix} A-\lambda I & B_2 \end{bmatrix}$ has full row rank for all $\mathrm{Re}\lambda \geq 0$. The second part implies that the matrix $\begin{bmatrix} A-\lambda I \\ C_2 \end{bmatrix}$ has full column rank for all $\mathrm{Re}\lambda \geq 0$.

(ii) $D_{12}$ has full column rank with $\begin{bmatrix} D_{12} & D_{\perp} \end{bmatrix}$ unitary, and $D_{21}$ has full row rank with $\begin{bmatrix} D_{21} \\ \tilde{D}_{\perp} \end{bmatrix}$ unitary.

(iii) $\begin{bmatrix} A-j\omega I & B_2 \\ C_1 & D_{12} \end{bmatrix}$ has full column rank for all $\omega$.

(iv) $\begin{bmatrix} A-j\omega I & B_1 \\ C_2 & D_{21} \end{bmatrix}$ has full row rank for all $\omega$.

The first assumption (i) is required for the stabilizability of $P$ by output feedback. The rank assumptions (ii) guarantee that the $H_2$ optimal control problem is nonsingular. In other words, they ensure that the controllers are proper and hence realizable. The unitary assumptions are made for the simplicity of the final solution, but they are not restrictions. Assumptions (i), together with (iii) and (iv), guarantee that the two Hamiltonian matrices associated with the $H_2$ problem, $H_2$ and $J_2$, belong to *dom(Ric)* (see also section 4.5). They ensure that the optimal controller $K$ does not try to cancel poles or zeros on the imaginary axis, which would result in closed-loop instability.

## 4.2. The augmented plant

In order to write the system in the format specified by figure 4-1, an augmented plant $P$ has to be built from the blockdiagram in figure 2-3. The first step in building the augmented plant is identifying the elements of the vectors $\underline{w}$, $\underline{z}$, $\underline{y}$ and $\underline{u}$ described in section 4.1. Since no reference signal or setpoint is used in this project, the only exogeneous input of the system, and therefore the only element of the vector $\underline{w}$ is the disturbance $d$. The vector $\underline{z}$ with 'error' signals has two elements of which the first one is the weighted control effort $\tilde{u}$. By weighing the control effort $u$ with a weighting filter $W_u$, the weighted control effort $\tilde{u}$ can be forced to have a high value at the frequencies of the disturbances to be suppressed and a low value at other frequencies. The second element of the vector $\underline{z}$ is the weighted output signal $\tilde{y}$. The output signal $y$ has to be weighed by a weighting filter $W_2$ that has no throughput term, i.e. the $D$ matrix in the state space notation of $W_2$ has to be zero, in order to fulfill assumption (ii) of section 4.1. The vectors $\underline{y}$ and $\underline{u}$ both only have one element, which are the output signal $y$ and the control effort $u$ respectively.
Now that all signals and weighting filters have been identified, the augmented plant can be constructed and is shown in figure 4-2.

[2] *A system P(s) is strictly proper when P(s) → 0 for s → ∞.*

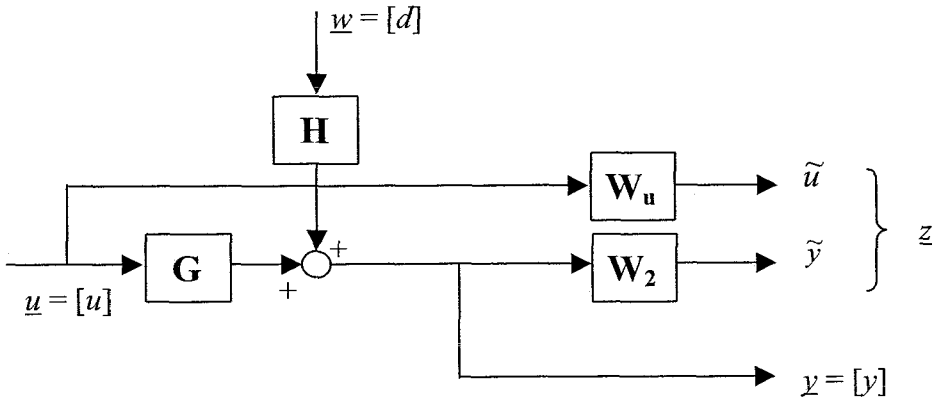


*figure 4-2: The augmented plant of the system*

## 4.3. Choice of the weighting filters $W_2$ and $W_u$

### *4.3.1. The weighting filter $W_2$*

As already mentioned in section 4.2 the filter $W_2$ is not allowed to have a throughput term in order to fulfill assumption (ii) of section 4.1. Therefore $W_2$ is chosen to be a first order lowpass filter with a cut-off frequency of $40 \cdot 10^3$ [Hz] and a static gain of 0 [dB]. The choice for a first order filter is made in order keep the final order of the controller $K$, which is the sum of the orders of all subsystems in the augmented plant, as low as possible. The cut-off frequency is chosen to be large so that it does not influence the shape of the controller for frequencies where noise has to be suppressed. The weighting filter $W_2$ is depicted in figure 4-3.

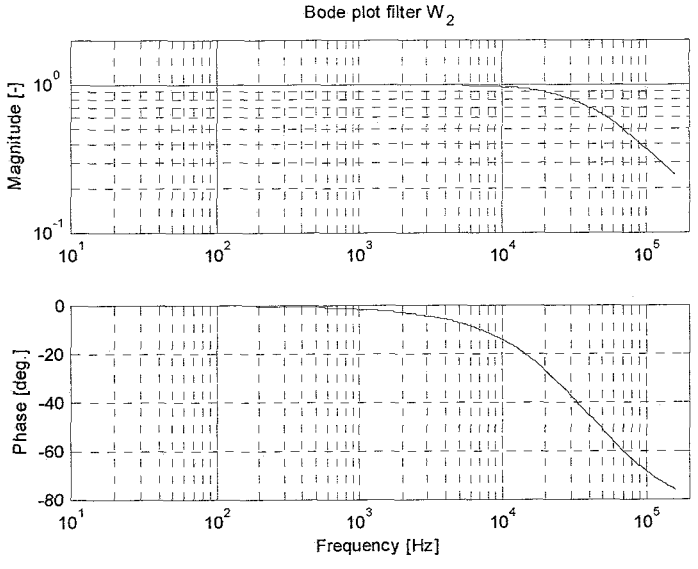


*figure 4-3: Amplitude and phase plot of the 1st order weighting filter $W_2$.*

### 4.3.2. *The weighting filter $W_u$*

As already mentioned in section 4.2, the weighting filter $W_u$ can be used to force the control effort to have a high value at the frequencies of the disturbances to be suppressed and a low value at other frequencies. However, this filter cannot be used to adjust the controller to cancel disturbances at different frequencies (see also section 6.2). Because the controller has to roll off at high frequencies, the shape of $W_u$ is chosen to be a high pass filter with three zeros at 160 [Hz], three poles at $12 \cdot 10^3$ [Hz] and a high frequency gain of 3.5 [-], as can be seen in figure 4-4. The order of the filter $W_u$ is chosen to be low to keep the eventual order of the controller $K$ as low as possible.

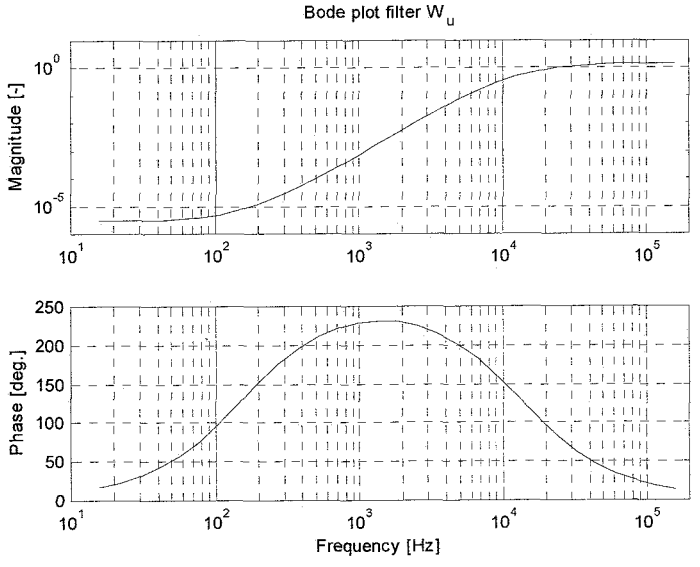


*figure 4-4: Amplitude plot (top) and phase plot (bottom) of the 3th order weighting filter $W_u$.*

## 4.4. The $H_2$ norm of the system

As outlined in section 4.1 the system $P$ is strictly proper because $D_{11}$ and $D_{22}$ are assumed to be zero. Then for the calculation of the $H_2$ norm of $P(s)$ the Frobenius norm[3] is used and integration takes place over the frequencies, as shown in equation (4-4).

$$\|P(s)\|_2 \stackrel{\Delta}{=} \sqrt{\frac{1}{2\pi}\int_{-\infty}^{\infty} tr\left(P(s)^H \cdot P(s)\right) d\omega} \qquad (4\text{-}4)$$

From this equation it can be seen that $P(s)$ has to be strictly proper, otherwise the $H_2$ norm is infinite. The factor $1/\sqrt{2\pi}$ is only introduced to get consistency with the 2-norm of the corresponding impulse response (see [10]). When the Frobenius norm is written in terms of singular values, which tell something about the gain of the system, the $H_2$ norm of the system $P(s)$ can also be written in terms of these singular values, as shown in equation (4-5).

---

[3] *The frobenius matrix norm (or Euclidean norm) is the square root of the sum of the squared element magnitudes* $\|A\|_F = \sqrt{\sum_{i,j} |a_{ij}|^2} = \sqrt{tr\left(A^H \cdot A\right)}$, *where $A^H$ is the complex conjugate transpose of A.*

$$\|P(s)\|_2 = \sqrt{\frac{1}{2\pi}\int_{-\infty}^{\infty}\sum_i \sigma_i^2(P(j\omega))d\omega} \tag{4-5}$$

From this equation it can be seen that minimizing the $H_2$ norm corresponds to minimizing the sum of the square of all the singular values ('gains') over all frequencies. Applying the $H_2$ norm to the standard block diagram of figure 4-1, where the augmented plant $P$ is given by figure 4-2, it can be seen that for the computation of the controller $K$ the $H_2$ norm of the transfer function matrix $T_{zw}$ (see equation 4-6) of the vector $\underline{z}$ to the vector $\underline{w}$ has to be minimized:

$$T_{zw} = \begin{bmatrix} \frac{HKW_u}{1-KG} \\ \\ \frac{HW_2}{1-KG} \end{bmatrix} \tag{4-6}$$

This transfer function matrix shows that in the design of the controller the weighting filter $W_u$ will have a limited contribution, since it only appears in one of the two transfer functions. The noise filter $H$, on the contrary, appears in both transfer functions in the matrix and therefore has a significant influence on the shape of the controller.

## 4.5. Computing the unique optimal controller

Once the assumptions described in section 4.1 have been satisfied, an optimal $H_2$ controller $K$ can be computed. First the solutions to two Riccati equations are computed. These two Riccati equations can be derived from the Hamiltonian matrices given by equation (4-7) and (4-8).

$$H_2 = \begin{bmatrix} A & 0 \\ -C_1^T C_1 & -A^T \end{bmatrix} - \begin{bmatrix} B_2 \\ -C_1^T D_{12} \end{bmatrix} \begin{bmatrix} D_{12}^T C_1 & B_2^T \end{bmatrix} \tag{4-7}$$

$$J_2 = \begin{bmatrix} A^T & 0 \\ -B_1 B_1^T & -A \end{bmatrix} - \begin{bmatrix} C_2^T \\ -B_1 D_{21}^T \end{bmatrix} \begin{bmatrix} D_{21} B_1^T & C_2 \end{bmatrix} \tag{4-8}$$

The derivation of the two Riccati equations is discussed in [9] and they are given by equation (4-9) and (4-10).

$$\left(A^T - C_1^T D_{12} B_2^T\right)X + X\left(A - B_2 D_{12}^T C_1\right) + X\left(-B_2 B_2^T\right)X + C_1^T C_1 - C_1^T D_{12} D_{12}^T C_1 = 0 \tag{4-9}$$

$$\left(A - B_1 D_{21}^T C_2\right)Y + Y\left(A^T - C_2^T D_{21} B_1^T\right) + Y\left(-C_2^T C_2\right)Y + B_1 B_1^T - B_1 D_{21}^T D_{21} B_1^T = 0 \tag{4-10}$$

The solutions to equations (4-9) and (4-10) are $X$ and $Y$ respectively, and they are denoted by $X = Ric(H_2)$ and $Y = Ric(J_2)$. The matrices $H_2$ and $J_2$ for which $X$ and $Y$ are defined, belong to $dom(Ric)$, which is the domain of the Riccati operator.

With the obtained solutions $X$ and $Y$, the unique optimal controller $K$ can be computed as shown in [9]. Because the fit of the plant $G$ is of $10^{th}$ order, the fit of the noise filter $H$ is of $4^{th}$ order, $W_2$ a $1^{st}$ order lowpass filter and $W_u$ is a $3^{rd}$ order highpass filter, the computed stabilizing controller is of $18^{th}$ order. To avoid numerical problems with the discretization described in section 4.6 the controller is reduced to $10^{th}$ order using a closed loop balanced model reduction technique [12].

## 4.6. Discretizing the controller

To implement the computed controller into the system, it first has to be discretized. The sampling frequency $f$ is chosen to be $45 \cdot 10^3$ [Hz], because at this frequency the $10^{th}$ order controller

can easily be computed in real time. To avoid as much high frequency phase shift as possible, since this phase shift may cause instability of the closed-loop system, the discrete time controller is not allowed to have a throughput term (see section 9: appendix 1). In order to achieve this, first the continuous time controller is written as a transfer function, shown in equation (4-11), where the zeros and poles are given by $z_i$ an $p_i$, respectively.

$$K(\omega)=\frac{(s-z_1)(s-z_2)...(s-z_{10})}{(s-p_1)(s-p_2)...(s-p_{10})} \tag{4-11}$$

Next the poles, thus the denominator of the continuous time controller, are converted to discrete time, using the equation (4-12):

$$p_{dt}=e^{p_{ct}\cdot T_s} \tag{4-12}$$

The discrete time transfer function of the controller is shown in equation (4-13), where the parameters $b_i$ have to be determined.

$$K(e^{i\omega})=\frac{num(e^{i\omega},\theta_b)}{den(e^{i\omega},\theta_a)}=\frac{b_0+b_1e^{-i\omega}+...+b_9e^{-9i\omega}}{1+a_1e^{-i\omega}+...+a_{10}e^{-10i\omega}} \tag{4-13}$$

Since the controller is not allowed to have a throughput term, one step time delay is introduced into the controller. Therefore one zero is lost and the order of the polynomial in the numerator is one degree lower than the order of the polynomial in de denominator. The numerator of the discrete time transfer function of the controller is now estimated using a least squares technique, in which the 2-norm of the difference between the discrete and continuous time controller is minimized:

$$\begin{aligned}\left\|K(e^{i\omega})-K(\omega)\right\|_2&=\left\|\left|\frac{1}{den(e^{i\omega},\theta_a)}\right|\left|num(e^{i\omega},\theta_b)-\tilde{K}(\omega)\right|\right\|_2\\&=\left\|W_1(e^{i\omega})\left|num(e^{i\omega},\theta_b)-\tilde{K}(\omega)\right|\right\|_2\end{aligned} \tag{4-14}$$

with

$$\tilde{K}(\omega)=K(\omega)den(e^{i\omega},\theta_a) \tag{4-15}$$

In equation (4-14), $num(e^{i\omega},\theta_a)$ is the numerator of the discrete time controller to be fitted to $K(\omega)den(e^{i\omega},\theta_a)$ and $W_1(\omega)$ is the first of two weighting functions used. Since it is built from de denominator of the transfer function of the discrete time controller, it is already known.
Eventually the sensitivity functions computed with both the continuous and discrete time controllers are desired to be the same, because these functions reflect the noise reduction achieved. Therefore a second weighting function is introduced, which is computed from the difference between these sensitivity functions:

$$\begin{aligned}&\left(\frac{1}{1-G_m(\omega)K(\omega)}\right)-\left(\frac{1}{1-G_m(\omega)K(e^{i\omega})}\right)\\&=\left(\frac{G_m(\omega)}{(1-G_m(\omega)K(\omega))(1-G_m(\omega)K(e^{i\omega}))}\right)(K(\omega)-K(e^{i\omega}))\\&=W_2(\omega)(K(\omega)-K(e^{i\omega}))\end{aligned} \tag{4-16}$$

Since $K(e^{i\omega})$ is not known yet, it is assumed that $K(\omega) = K(e^{i\omega})$, and the weighting function $W_2(\omega)$ is shown in equation (4-17).

$$W_2(\omega)=\frac{G_m(\omega)}{(1-G_m(\omega)K(\omega))^2} \tag{4-17}$$

Using the weighting functions $W_1(\omega)$ and $W_2(\omega)$, the numerator of the discrete time controller is estimated with a discrete time least squares estimation technique. The resulting $10^{th}$ order discrete time controller is depicted in figure 4-5, together with the original continuous time controller.

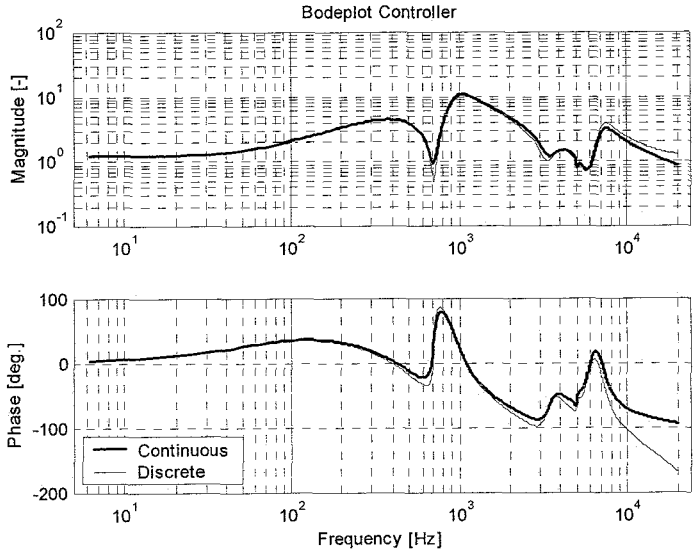


*figure 4-5: Amplitude and phase plot of $10^{th}$ order continuous time controller (thick line) and resulting $10^{th}$ order discrete time controller (thin line).*

From this figure it can be seen that for high frequencies the discrete time controller does not roll off as much as the continuous time controller and that some phase shift occurs because of the discretization. This is due to the fact that the discrete time controller has one zero less than the continuous time controller and therefore a perfect fit can never be obtained.

## 4.7. Implementation results

When the designed and discretized controller is implemented into the real system, extra phase shift occurs because of sampling (see section 9: appendix 1). This extra phase shift, however, does not destabilize the closed loop system, as can be seen from
figure 4-6. In the Nyquist plot depicted, it can be seen that the phase margin resulting from the computed controller and the measurement data of the plant $G$ is approximately 60 [deg]. The phase margin computed from the closed loop measurement of the senstivity function $S$ is a little smaller, but still large enough to guarantee stability: about 50 [deg].

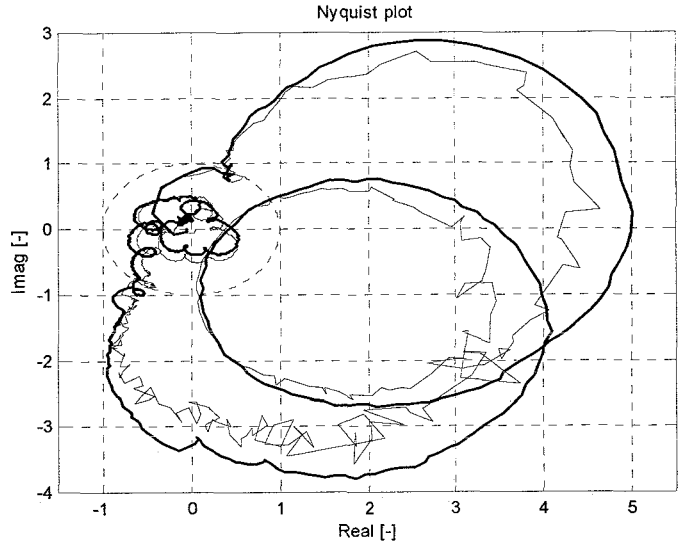


*figure 4-6: Nyquist plot of loopgain L(ω) for L(ω)=-(1-1./S(ω)) (thin line) and L(ω)=G(ω)K($e^{i\omega}$) (thick line), where S(ω) is the measured sensitivity function, $G(\omega)=\hat{G}(\omega)$ and K($e^{i\omega}$) is the 10$^{th}$ order discretized feedback controller.*

The above mentioned measured sensitivity function

$$S=\frac{1}{1-GK} \tag{4-18}$$

is depicted in figure 4-7, together with the sensitivity function computed from the model $G_m$ and the discretized 10$^{th}$ order controller from section 4.6. The measured sensitivity function shows that noise reduction takes places in the frequency range of $30 - 2{\cdot}10^3$ [Hz]. The peak in the sensitivity function at $f$ = 600 [Hz] can be explained from the dip in the model $H_m$ at $f$ = 600 [Hz] (see also section 3.3). From figure 4-7 it can also be seen that the measured sensitivity differs significantly from the model sensitivity until 300 [Hz] and that not all high frequent resonance modes are fitted exactly. This can be explained by the fact that the model $G_m$ differs from the plant $G$.

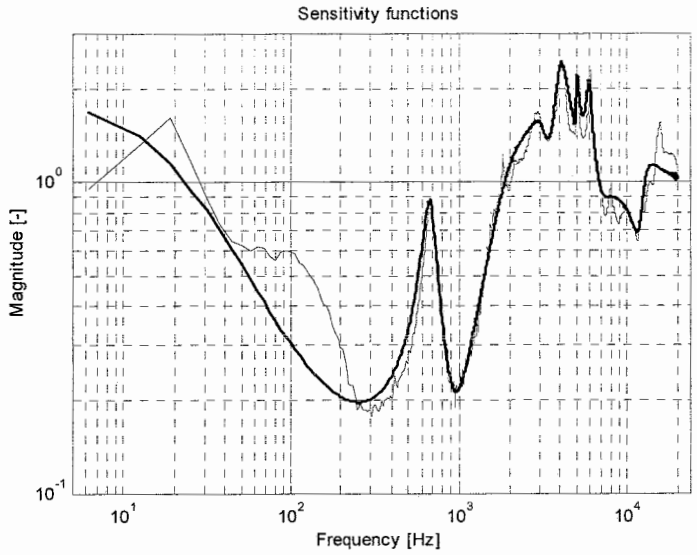


*figure 4-7: Measured sensitivity function (thin line) and sensitivity function computed from the model $G_m$ of the plant G and the discretized $10^{th}$ order feedback controller (thick line).*

Figure 4-8 shows the original frequency response data of the (open loop) noise filter $H$, together with the process sensitivity function:

$$H_{cl} = \frac{H}{1 - GK} \tag{4-19}$$

which indicates the noise reduction achieved using the controller $K(e^{i\omega})$. Also from this figure it can be seen that noise cancellation takes place in the frequency range of $30 - 2 \cdot 10^3$. [Hz].

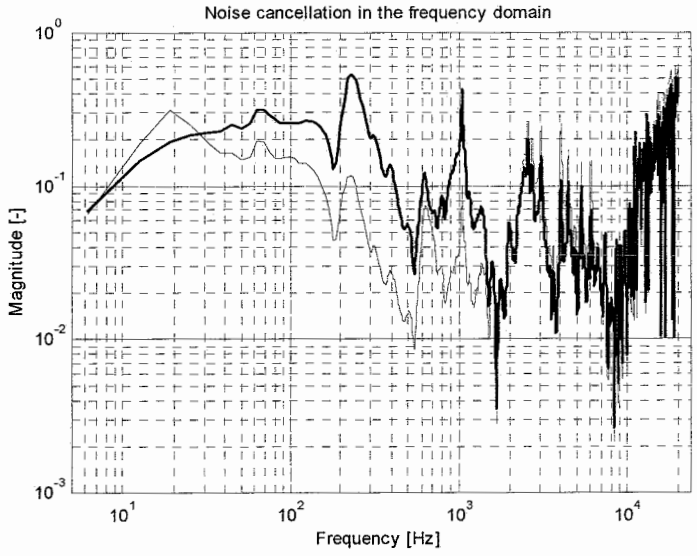


*figure 4-8: Noise cancellation in the frequency domain. The thin line shows the closed loop transfer function $H_{cl} = H(1-GK)^{-1}$ with $10^{th}$ order discrete time feedback controller. The thick line shows the case without control, i.e. $H_{cl}=H$.*

# 5. Controller relevant modeling for ANC

## 5.1. Controller relevant modeling

Now that the controller $K(\omega)$ is known, controller relevant modeling, as it is described in section 3.4, can be applied. The used weighting function is shown in
figure 5-1, together with the frequency response data of the plant $G$ and the weighting function relative to uniform weighting:

$$W_r(\omega)=\frac{W(\omega)}{1/G(\omega)}=W(\omega)G(\omega) \tag{5-1}$$

From the relative weighting function in this figure it can be seen that weighing low frequencies is important, as well as weighing the resonance peaks around $f = 4 \cdot 10^3$ [Hz]. On the other hand, the high frequency area ($f > 6 \cdot 10^3$ [Hz]) is not important at all.

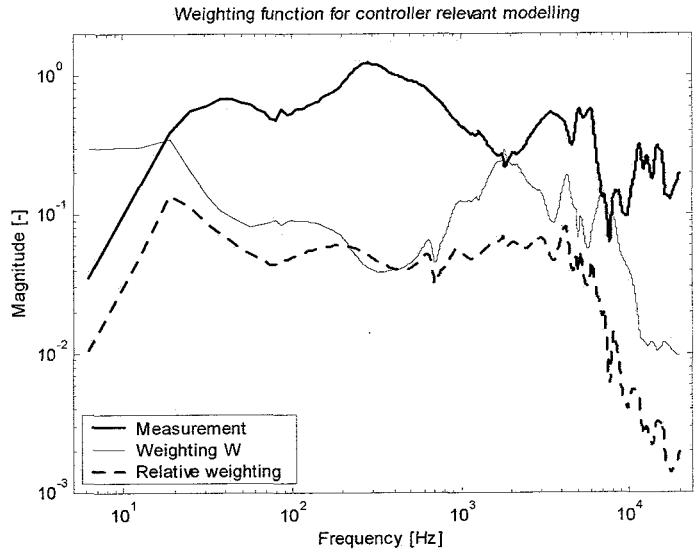


*figure 5-1: Amplitude plot of the frequency response data of the plant G (thick line), the weighting function W (thin line) and the relative weighting function (dotted line).*

Using the weighting function from equation (3-3), a $12^{th}$ order fit of the plant $G$ is obtained which is shown in
figure 5-2, together with the initial fit and the frequency response data of the plant $G$. This figure shows that indeed the fit is improved at low frequencies and deteriorated in the high frequency area.

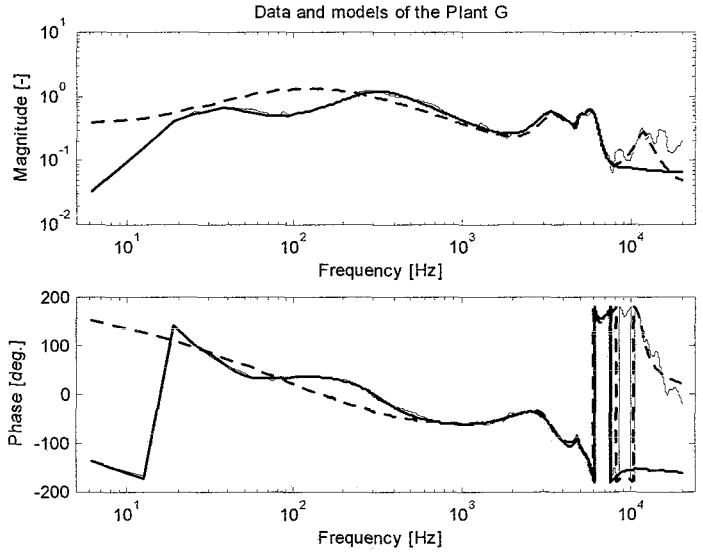


*figure 5-2: Amplitude and phase plot of the frequency response data of the plant G (thin line), the original model (dotted line) and the fitted model after one iteration step (thick line).*

## 5.2. Control design and implementation

Once the new model of the plant $G$ is obtained, a new controller can be computed, using the same weighting filters as described in section 4.3. The obtained continuous time controller is reduced to $11^{th}$ order, again using the closed loop balanced model reduction technique [12] mentioned in section 4.5 and it is shown in
figure 5-3, together with the initial $10^{th}$ order controller. This figure shows that the controllers are more or less the same at high frequencies, but at low frequencies the gain of the controller after the iteration step is much bigger than the gain of the initial controller. This is the result of the fact that for low frequencies the gain of the second model $G_m$ is much lower than that of the initial model.

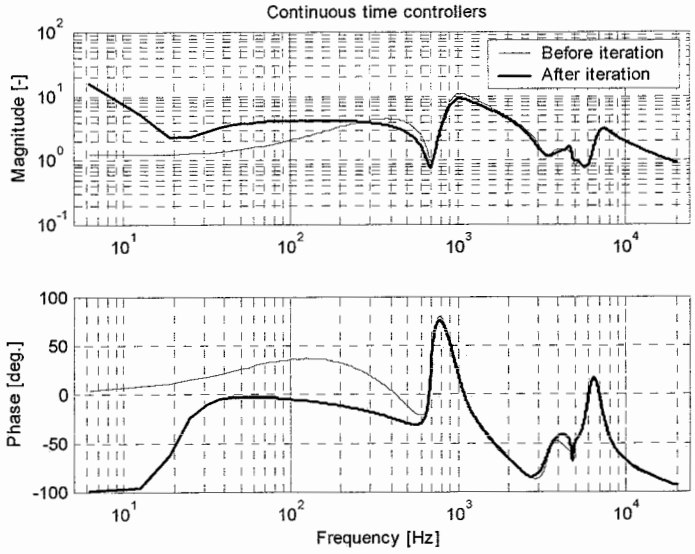


*figure 5-3: Amplitude and phase plot of the initial $10^{th}$ order continuous time controller (thin line) and the $11^{th}$ order continuous time controller after the iteration step (thick line).*

After computing the continuous time controller, it is discretized as described in section 4.6. After implementing the controller, a sensitivity function is measured which is compared with the model sensitivity function in figure 5-4.

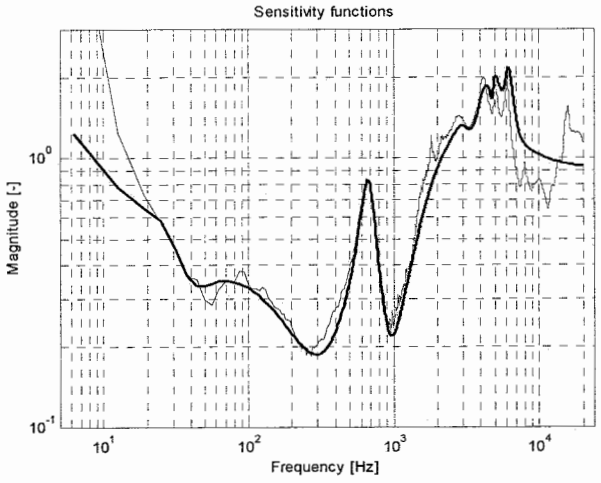


*figure 5-4: Measured sensitivity function (thin line) and sensitivity function computed from the model $G_m$ after the iteration step and the discretized $11^{th}$ order controller (thick line).*

From this figure it can be seen that also for low frequencies the sensitivity based on the model resembles the measured sensitivity quite well. Note that the measured data below $f = 20$ [Hz] cannot be trusted, since the coherence function between input and output was very low. In figure 5-5 the measured sensitivity based on the initial model of the plant and the one based on the model after the iteration step are compared. It can be seen that after the iteration step more noise reduction takes place in the frequency domain between 15 and 200 [Hz].

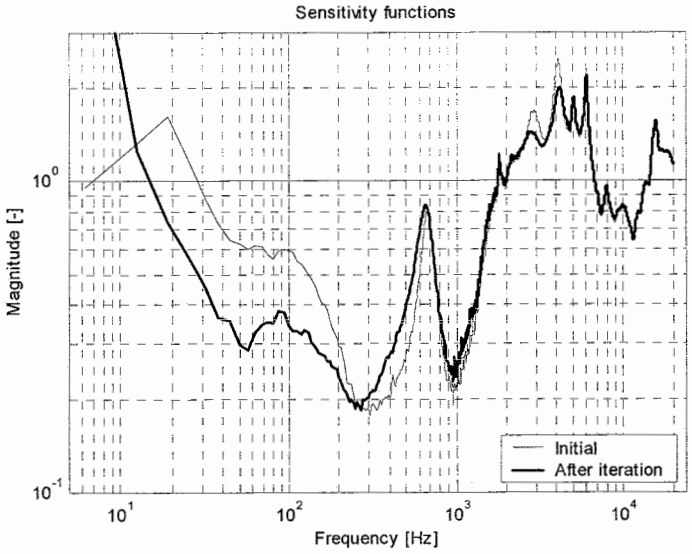


*figure 5-5: Measured sensitivity functions based on initial model $G_m$ and resulting initial controller (thin line) together with model $G_m$ after iteration step and resulting controller (thick line).*

# 6. Adjustability of the controller

## 6.1. Goals of adjustability

As mentioned before, the use of digital controllers comes with some disadvantages, but also with many advantages. In this section, the ease of adjustment of software parameters of digital controllers is exploited. Since it is relatively easy to change filter coefficients 'on line', the user of the headset could be given the ability to adjust the controller to suit his or her needs. For example, the headset could be equipped with a dial to let the user choose the frequency range in which the controller should reduce environmental noise.
In this section, an attempt is made to parameterise the controller, so its effective noise reduction frequency range becomes dependent on one parameter – in this case $\delta$.

## 6.2. Application of parameterisation to the augmented plant

In section 4.4 it was shown that the shape of the controller is much more dependent on the shape of the noise filter $H$ than on the shape of the weighting filter $W_u$. In fact, the noise model $H$ is nothing more than just another weighting function in the augmented plant of the $H_2$ control problem. Because of this sensitivity, it is a logical place to start when examining the possibility of parameterizing the controller.

## 6.3. Construction of a suitable noise filter *H*

### *6.3.1. Basic shape of the noise filter*

Since the noise model $H$ actually defines the frequency shape of the present noise, in a frequency range where its amplitude response is high, the $H_2$ control problem would try to put more control effort in reducing the noise, thus letting the amplitude response of the controller become higher. Some experiments showed that a suitable shape for $H$ is a hat-like shape, made up by a $4^{th}$ order transfer function as depicted in figure 6-1. This 'hat' will then be moved along the frequency axis, in order to force control effort to be mainly inside the 'hat'.

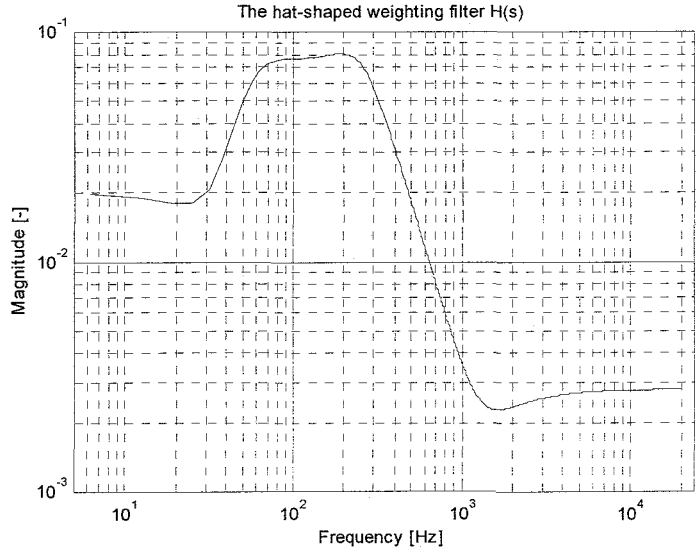


*figure 6-1: Amplitude plot of the hat-like shape of the proposed noise filter H*

### 6.3.2. *Restrictions*

When moving the hat-like shape of $H_m$ along the frequency axis, some properties of the system have to be considered. Because the speaker/microphone combination inside the ear cups of the headset cannot produce or pick up frequencies below 100 [Hz], it would be useless to create a weighting filter $H_m$ that has a high gain in this range.
An upper bound for the high-gain frequency range of $H_m$ comes from non-minimum phase zeros in the plant $G$. Since every model of $G$ has one real and two complex conjugate non-minimum phase zeros at about 12 [kHz], they are likely to be a property of the real system. From properties of the Bode-sensitivity integral, it follows that these zeros restrict the maximum achievable bandwidth to a frequency well below the non-minimum phase zeros. Trying to push the maximum of the weighting filter $H_m$ too close to this frequency would cause high peaks in the sensitivity, eventually letting the closed loop system become practically unstable.
Since the goal of the investigation of a possible parameterisation of the controller is not to achieve noise reduction for frequencies as high as possible, the upper frequency of the maximum gain of the weighting filter $H$ will be limited accordingly.

### 6.3.3. *Application*

First, a transfer function is created, showing a hat-like shape in the amplitude-plot. In order to move this hat-like shape, this 4th order transfer function has to be parameterised, dependent on the parameter $\delta$:

$$\left.\begin{aligned} \omega_1 &= 64\pi + 1000\delta \\ \omega_2 &= \frac{57}{32}\omega_1 \\ \omega_3 &= 520\pi + 1000\delta \\ \omega_4 &= \frac{1241}{260}\omega_3 \end{aligned}\right\} \quad \delta = [0 \ldots 1] \tag{6-1}$$

$$H(s) = \frac{\left(\frac{1}{\omega_1^2}s^2 + \frac{2\beta_1}{\omega_1}s + 1\right)\left(\frac{1}{\omega_4^2}s^2 + \frac{2\beta_4}{\omega_4}s + 1\right)}{\left(\frac{1}{\omega_2^2}s^2 + \frac{2\beta_2}{\omega_2}s + 1\right)\left(\frac{1}{\omega_3^2}s^2 + \frac{2\beta_3}{\omega_3}s + 1\right)} \tag{6-2}$$

In equation 6-2, $\beta_1 \ldots \beta_4$ are the damping coefficients, in this case all fixed at 0.45 [-]. When parameterised like this, the frequency range where the magnitude of $H_m$ is high will move along the frequency axis linearly, keeping the maximum at a constant value. The width of this elevation will be constant only on a linear scale; on a logarithmic scale it will seem to become narrower for larger values of $\delta$. This will help to prevent the controller to push too high against the bandwidth-limiting, non-minimum phase zeros, avoiding sudden changes in the shape of the controller due to stability problems. Moreover, it will keep the frequency parameterisation fair, as the effective bandwidth is not widened. An amplitude-plot of the filter for $\delta$'s between 0 and 1 with increments of 0.1 can be seen in figure 6-2.

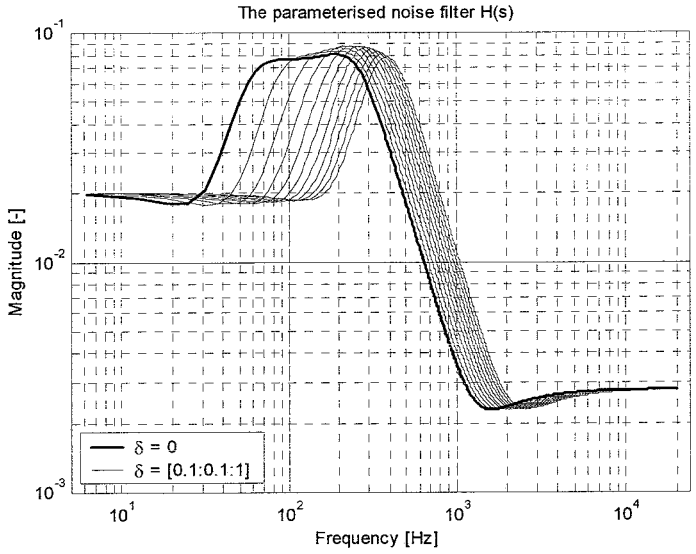


*figure 6-2: Amplitude plot of the parameterized weighing filter H*

## 6.4. Calculating the controllers

With the above parameterisation for the filter $H$, the initial $10^{th}$ order model $G_m$ and the weighting filters $W_2$ and $W_u$, as they are described in section 4.3, a number of controllers have been calculated for $\delta \in [0 \ldots 1]$ with increments of 5 $10^{-2}$ [-]. Since the discretization method discussed in section 4.6 requires the controller to be reduced in order, and also changes the position of the zeros of the controller, only continuous time controllers are evaluated here. Bode plots of the resulting $18^{th}$ order continuous time controllers are depicted in figure 6-3. As can be seen from this figure, only the low-frequency part of the controller $K(\omega)$ changes. In the high-frequency range, neither the amplitude nor the phase response of the controller changes significantly. This could imply that there are also but few poles and zeros that significantly depend on $\delta$.

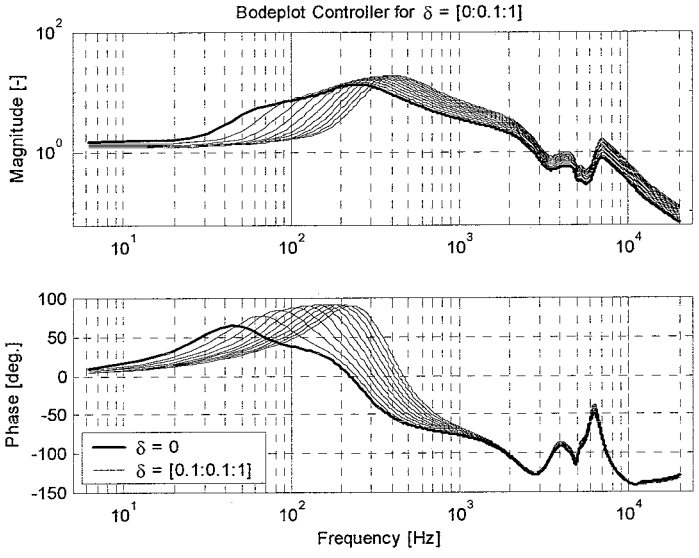


*figure 6-3: Amplitude and phase plot of the controllers for δ= [0:0.1:1]*

This can be investigated by looking at a plot of the poles and zeros in the complex plane. However, since it is not clear from this kind of plot what the dependency of the poles and zeros on the parameter $\delta$ is, the absolute values of the poles and zeros are plotted versus $\delta$ in figure 6-4 and figure 6-5 respectively. From these plots it becomes clear that there are only a few poles and zeros that change significantly with $\delta$, while most of the poles and zeros do not change at all. Note that since the controller changes only significantly in its low-frequency range, it can be expected that mainly the slower poles/zeros move. This effect can also be clearly seen in the figures below.

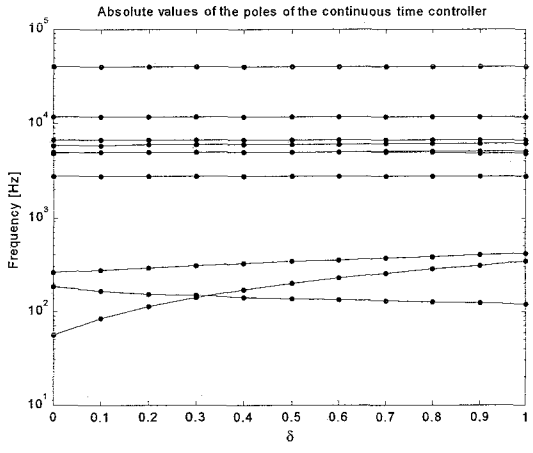


*figure 6-4: Absolute values of the poles of the continuous time controller versus the parameter $\delta$*

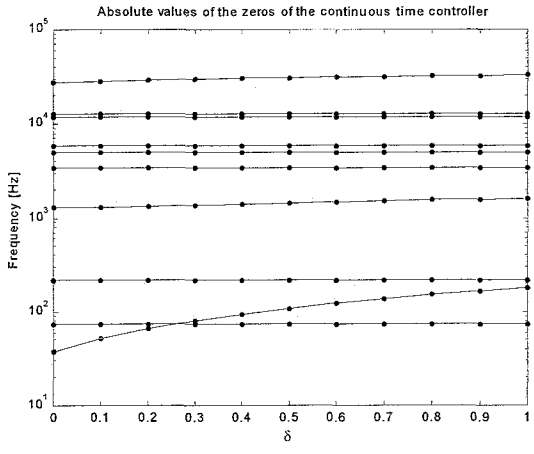


*figure 6-5: Absolute values of the zeros of the continuous time controller versus the parameter $\delta$*

In figure 6-6 the effect of the changing controller on the sensitivity function – computed from the frequency response function of the plant $G$ and the 18$^{th}$ order continuous time controller – can be seen, whereas in figure 6-7 the Nyquist plots of the loopgain computed from the model $G_m$ of the plant and the 18$^{th}$ order continuous time controller can be found to have sufficient gain/phase margins.

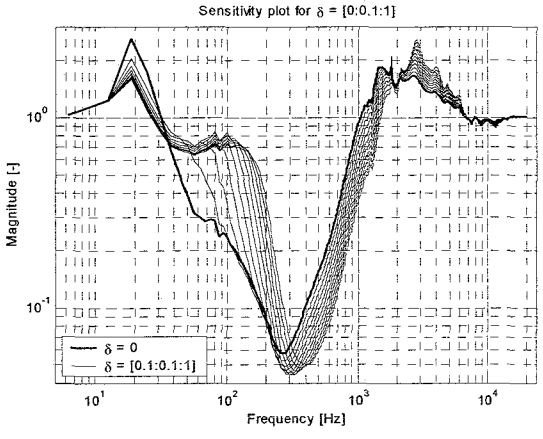


*figure 6-6: Sensitivity functions S=(1- G(ω)K(ω) where G(ω)= ( ω) and K(ω) is the 18$^{th}$ order continuous time controller, for δ=[0:0.1:1]*

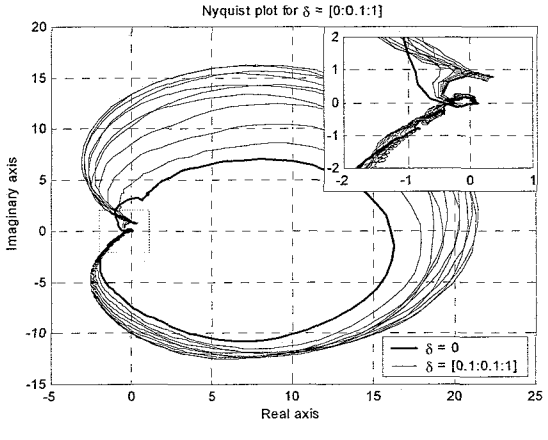


*figure 6-7: Nyquist plot of loopgain L(ω)=G(ω)K(ω) where G(ω) = $G_m$(ω) and K(ω) is the 18$^{th}$ order continuous time controller, for δ=[0:0.1:1]*

## 6.5. Evaluation

As was demonstrated in the previous sections, a dependency of the poles and zeros of the controller on the parameter $\delta$ can be found. In future research, this dependency could be fitted with a low order polynomial in order to be able to position the frequency range of noise reduction

continuously. However, this is not trivial, for as the absolute value of the poles and zeros moves smoothly with the parameter $\delta$, this is not the case for their position in the complex plane. Particularly the zeros tend to switch between real and complex conjugate positions without much coherence.
Moreover, the examination of the dependency on $\delta$ was done entirely in continuous time. In order to implement an adjustable controller, the parameterised controller has to be discretized, which is not a trivial conversion, for – as explained in section 4.6 – no throughput term should be present after discretization. Elimination of this throughput term requires the introduction of one step time-delay at the cost of one zero. As the zeros are then estimated with a non-linear least squares optimisation it becomes difficult to see a coherent course of change in the zeros of the discrete time controller.
Besides discretization problems, further effort should be made to gain controller performance by not only parameterizing the noise filter $H$, but also the effort weighting filter $W_u$. In this study, the effort weighting was not adjusted, whereas it is reasonable to assume that it would be of influence, since it weighs the control effort over the desired frequency range.

## 6.6. Implementation

In order to be able to show some results of the parameterisation, controllers for $\delta$=[0,0.5,1] have been implemented on the real system. Measured sensitivity plots can be found in figure 6-8. From this figure it can be seen that for $\delta = 0$ there is more noise reduction at low frequencies, whereas for $\delta = 1$ noise reduction takes place in the high frequency-area.

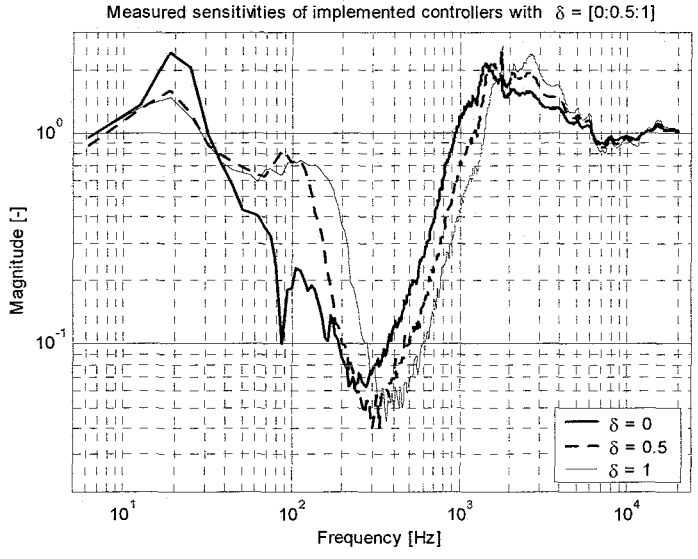


*figure 6-8: Measured sensitivity functions for implemented controllers with $\delta$=0 (thick line, $\delta$=0.5 (dotted line) and $\delta$=1 (thin line).*

# 7. Issues of application to people

During the entire process from model synthesis to controller calculation, use has been made of measurements in the experimental set-up. However, this set-up was based upon a dummy-head, made of styrofoam and plastics. A real head could possibly change the frequency response of the plant *G* significantly.
Because of the feedback techniques used, changes in the plant *G* will cause changes in the Nyquist-plot of the loop gain and in the sensitivity plot, and could have negative influence on the closed loop stability. Measurements on people could provide insight into necessary robustness.

## 7.1. The plant *G*

From practical experience it shows that the position of the headset on the head has a lot of influence on the transfer function of the plant *G*. It can also be safely stated, that the makeup of materials in the head, as well as its shape and the shape of the ear will also have influence on the frequency response of the plant *G*. In order to be able to make a statement on the robustness, experiments need to be done, applying the headset to the heads of people.
Measurements will be carried out in the same way as discussed in section 2.3, with the exception that the sound-isolated box will not be present, causing more disturbance to the measurements due to environmental noises. Three test-persons have worn the headset and the results of the conducted measurements are shown in figure 7-1. These measurements have made clear that the magnitude of the frequency response function of the plant G changes significantly in frequency areas that are important to closed loop stability, particularly in the 5 - 15 [kHz] range. The phase plots, however, are quite similar.

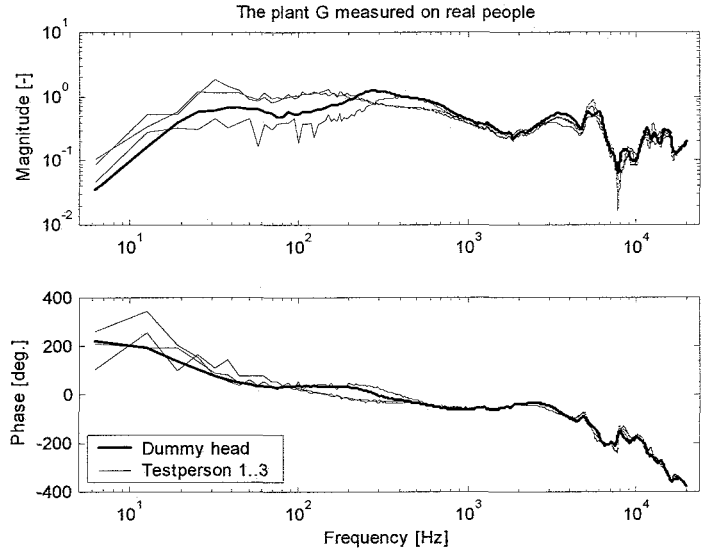


*figure 7-1: Amplitude and phase plot of the plant G, measured on 3 persons (thin lines), compared to the dummy head (thick line). In the lower frequency range, measurements should not be trusted due to low coherence. However, above 200 [Hz] coherence is high enough to state that the frequency response of the plant G changes significanty in areas relevant to closed-loop stability, i.e. approximately 5...15 [kHz].*

## 7.2. Stability

The significant changes in the frequency response of the plant $G$ will also affect the closed loop stability. In the figures below, a plot of the calculated sensitivity, next to a nyquist plot of the loop-gain are depicted. For these plots, the controller as obtained in section 5.2 was used. As can be seen in the sensitivity-plot in figure 7-2, the deviation of the frequency response of the plant $G$ around 8 [kHz] results in high spikes, proving this deviation to be significant and a possible threat to stability.

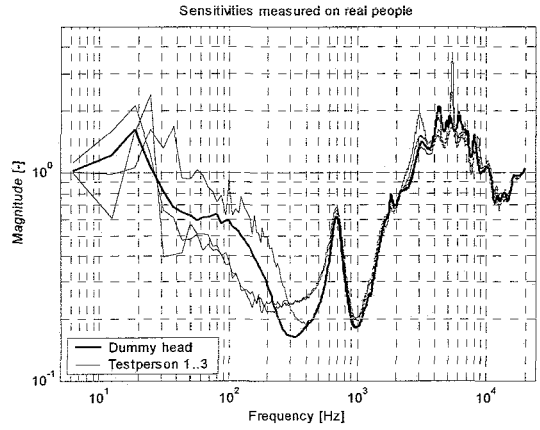


*figure 7-2: Sensitivity-plots using the original plant-measurements (thick line) and measurements on real persons (thin lines), based on the same loopgain as figure 7-3 . High spikes in high-frequent areas indicate large deviations to original measurements and possible threats to stability.*

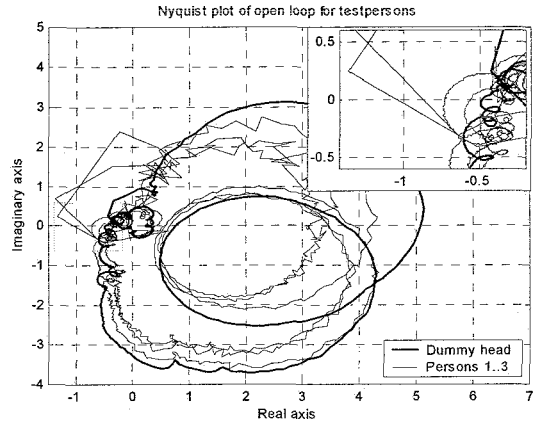


*figure 7-3: Nyquist plots of the loopgain $L(\omega)=G(\omega)K(e^{i\omega})$ where $G(\omega)=(\ \omega)$ based on the measurements on real persons (thin lines) and $K(e^{i\omega})$ is the discretized controller as obtained in section 5.2. Stability could be compromised for certain persons, but little weight should be applied to low frequency data, due to low coherence in measurements.*

The sensitivity-plots in figure 7-2 show little change in performance above approximately 600 [Hz], but significant changes below this frequency. However, from the Nyquist plot of the loop-gain depicted in
figure 7-3 it can be seen that the stability is not compromised in this high-frequency range, but – if at all – in the low frequency range. However, low frequency values in these plots cannot be trusted due to low coherence functions of the measurement data. The reason for this lack of coherence compared to previous measurements is twofold: the sound-isolated box, shielding the set-up from environment noises can not be used with test-persons, and in order to make the measurement not too unpleasant for the test-persons, the volume of the sound has been kept lower. Hence, no conclusions can be drawn to whether or not this compromises closed loop stability based on these plots, but in practice the controlled system proved to remain stable. It does point out however, that serious effort should be made to investigate where robustness is necessary and where peak-performance can be reached.

# 8. Conclusions and Recommendations

The results from this research project have shown that discrete time (digital) control techniques are suitable to be used for active noise control (ANC) purposes. Moreover, the model based $H_2$-approach has proven to provide stable controllers with adequate performance, comparable to the analogue commercial headset used. A controller relevant modelling step was also found to have a positive effect on noise reduction performance.
However, as has been shown in section 7, the plant $G$ changes quite significantly when applied to different persons. This calls for more research to provide information about the robustness necessary to create stable controllers for a wide public.
Secondly, the highest peaks in the sensitivity lie in an audible frequency range (around 5 [kHz]), resulting in a soft hissing sound. In commercial applications, this can of course not be permitted, but removing this hissing sound would reduce noise reduction performance. Moreover, in a commercial product, a reference signal would also be necessary – requiring for example system inversion techniques – that were beyond the scope of this research.
In section 6, it was shown that it could be possible to create a continuous time controller that has noise reduction, adjustable over a certain frequency range. As mentioned, creating a controller that is adjustable in discrete time would require overcoming a few major obstacles.

# References:


1. P.O.A.L. Davies and M.F. Harrison, *"Predictive acoustic modelling applied to the control of intake/exhaust noise of internal combustion engines"*, Journal of sound and vibration, vol. 202, no. 2, pp. 249-274, 1997

2. M.McJury, R.W.Stewart, D.Crawford and E.Toma, *"The use of active noise control (ANS) to reduce acoustic noise generated during MRI scanning: some initial results"*, Magnetic resonance imaging, vol. 15, no. 3, pp. 319-322, 1997

3. Jong-Yih Lin, Horng Sheu, *"Robust internal model-based LQG design for active noise control of a one-dimensional acoustic duct system"*, Optimal control applications & methods, vol. 20, pp. 267-282 (1999)

4. David S. Nelson, Scott C. Douglas and Marc Bodson, *"Fast and exact algorithms for feedforward active noise control"*, International journal of adaptive control and signal processing, vol. 14, pp. 643-661, 2000

5. Jcongho Hong, James C. Akers, Ravinder Venugopal, Miin-Nan Lee, Andrew G. Sparks, Peter D. Washabaugh and Dennis S. Bernstein, *"Modelling, identification and feedback control of Noise in an acoustic duct"*, IEEE Transactions on control systems technology, vol. 4, no. 3, May 1996

6. M.R. Bai and H.H. Lin, *"Comparison of active noise control structures in the presence of acoustical feedback by using the $H_\infty$ synthesis technique"*, Journal of sound and vibration, vol. 206, no. 4, pp. 453-471, 1997

7. M.R. Paurobally and J. Pan, *"The mechanisms of passive eardefenders"*, Applied acoustics, vol. 60, pp. 293-311, 2000

8. Angela Kuo Wang and Benedict Tse, *"Adaptive active noise control for headphones using the TMS320C30 DSP"*, SPRA160, Texas Instruments, January 1997

9. K. Zhou, J.C. Doyle and K. Glover, *"Robust and optimal control"*, ISBN 0-13-456567-3, New Jersey, 1996

10. S.Skogestad and I.Postlethwaite, *"Multivariable feedback control"*, ISBN 0-471-94277-4, 0-471-94330-4, Chichester, November 1997

11. BOSE® Corporation, *http://www.bose.com/noise_reduction/personal/qc_headset/tech.html*

12. R.A. de Callafon, *"Closed loop balanced model reduction technique"*, Delft University of Technology-WbMt, 1995

# 9. Appendix 1: Delays due to discretization

As discussed in section 4.6, the controller needs to be discretized in order to be able to implement it onto the real system. However, because of this discretization, the implemented discrete time controller will be inherently different from the continuous time controller.
Besides small changes in the overall shape of the frequency response of the controller, a phase delay is inherently introduced when the controller is implemented. This delay cannot be seen in a bode-plot of the discretized controller (unless it is compensated), and is composed of two elements. In this appendix those two components will be explained in more detail.

## 9.1. Introduction

A digital controller keeps repeating the following steps for each sample: data acquisition (A/D conversion), calculation and voltage output (D/A conversion). Every step takes a small amount of time to complete, and – with some exceptions – they have to be completed sequentially. This is explained in figure 9-1. Let $t_0$ be the time at which the A/D conversion is started. Then $t_1$ is the time when this is complete and calculations can begin. At $t_2$ the calculations are finished and at $t_3$ the resulting voltage value will be output to the D/A converter. This last action takes until $t_4$, when the cycle is complete.

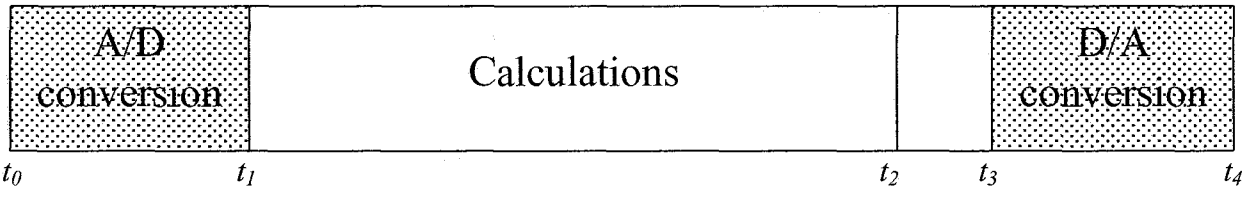


*figure 9-1: Time-line of a cycle of an implemented discrete time controller.*

In the case of this active noise control project, the calculation step takes up almost all of the time between two samples ($T_s$), because of limited computing power and high sampling rates. The moment at which the result of a calculation will be sent to the D/A converter will therefore be timed so that the D/A conversion will be finished when the next sample is due. Idle time will therefore exist between $t_2$ and $t_3$, and if the D/A conversion is timed right, $t_4$ will match $t_0$ for the next sample.

## 9.2. Throughput terms

A problem occurs with the implementation of a discrete time controller that has a throughput term, i.e. a non-zero $D$-matrix in state-space notation. In this case, a measured state should be accounted for in calculations and made available to the output at exactly the time at which the measurement was done. However, since calculations and both A/D and D/A conversions take time, this cannot be practically realised. Implementing a controller with a throughput term would cause serious deformation of the frequency response of the controller. Since the throughput term cannot be accounted for earlier than the time it takes for the calculations and both the A/D and D/A conversions to complete, this will be the delay to be introduced on implementation. If no changes are made to the way in which A/D and D/A conversions are timed (i.e. the D/A conversion finishes when a new sample is due), the phase delay introduced by the throughput term will reach 360° at the sampling frequency and therefore 180° at the Nyquist frequency.

## 9.3. Quantization in the time-domain

The second component in the extra phase-delay is caused by the discretization itself. If a control signal becomes available only at fixed time-intervals, and is held unchanged during the intervals (zero order hold), then the signal has an effective time-delay of half this time-interval. This is clarified in figure 9-2.

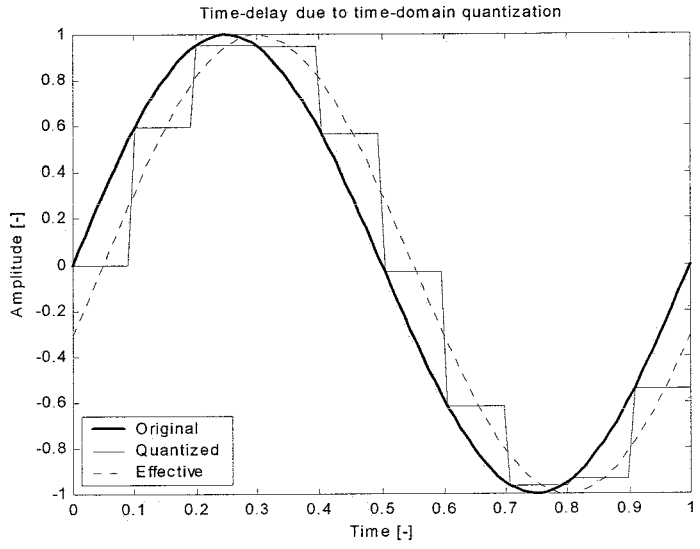


*figure 9-2: Delay introduced by quantization in time-domain. If the output value is only known at fixed intervals, it lags behind everywhere but on those intervals, causing an effective delay of half the time-interval.*

## 9.4. The total time-delay

Summarizing, the time-delay $\Delta T$ introduced by implementation of a discrete time controller with sample time $T_s$ can be expressed as:

$$\begin{cases} \Delta T = \dfrac{T_s}{2} & \text{Without throughput term} \\ \Delta T = \dfrac{T_s}{2} + T_{A/D} + T_{calc} + T_{D/A} = \dfrac{T_s}{2} + T_{tp} & \text{With a throughput term} \end{cases}$$

Written as a function of the frequency $f$, the introduced phase-delay becomes:

$$\begin{cases} \Delta\varphi = \pi f T_s & \text{Without throughput term} \\ \Delta\varphi = \pi f (T_s + 2T_{tp}) & \text{With a throughput term} \end{cases}$$